Squeezing Multilevel Atoms in Dark States via Cavity Superradiance

Bhuvanesh Sundar,* Diego Barberena, Ana Maria Rey, and Asier Piñeiro Orioli
JILA, NIST, Department of Physics, University of Colorado, Boulder, Colorado 80309, USA
and Center for Theory of Quantum Matter, University of Colorado, Boulder, Colorado 80309, USA

(Received 28 February 2023; revised 13 August 2023; accepted 19 September 2023; published 17 January 2024)

We describe a method to create and store scalable and long-lived entangled spin-squeezed states within a manifold of many-body cavity dark states using collective emission of light from multilevel atoms inside an optical cavity. We show that the system can be tuned to generate squeezing in a dark state where it will be immune to superradiance. We also show more generically that squeezing can be generated using a combination of superradiance and coherent driving in a bright state, and subsequently be transferred via single-particle rotations to a dark state where squeezing can be stored. Our findings, readily testable in current optical cavity experiments with alkaline-earth-like atoms, can open a path for dissipative generation and storage of metrologically useful states in optical transitions.

DOI: 10.1103/PhysRevLett.132.033601

Subradiant states that emit light at a rate slower than independent atoms because of (quantum) interference [1], have attracted widespread interest owing to their potential applications in quantum memories [2], mirrors [3,4], excitation transport [5,6], topological physics [7–11], entangled photons [12], and quantum metrology [13–16]. A long-standing challenge is finding simple ways to prepare target many-body subradiant states with useful properties such as scalable entanglement, i.e., entanglement which increases with system size. Optical cavities have demonstrated the capability to create *collective* (i.e., fully symmetric) quantum many-body states with scalable entanglement in the form of squeezing [17–23]. However, creating optically excited entangled states that are immune to collective dissipation and metrologically useful has remained a major challenge.

In generic atom-cavity experiments with two-level atoms, collective states are typically not dark but superradiant [1,24,25]. One way to stabilize the decay and create scalable entanglement is by using an additional coherent drive which competes with superradiance [26–35]. However, after turning off the drive, excited atoms superradiantly decay to the ground state, and the entanglement is destroyed.

Here, we propose to use *multilevel* atoms coupled to a dissipative cavity [see Fig. 1(a)] to generate scalable squeezing in two distinct modes and store it in dark states, recently shown to exist in these systems [36–38]. At the mean-field level, these dark states can be understood as the cancellation of the collective dipoles corresponding to different internal atomic transitions, see orange arrows in Fig. 1(b). In the full quantum theory, however, these dark states are necessarily entangled, as revealed by their squeezed fluctuations, and are hence absent in single atoms. We focus on effective four-level atoms [Fig. 1(b)] and describe two cases: one where collective decay generates squeezing in a dark state directly, and one where squeezing is created in a bright state due to a combination of superradiance and coherent driving. For the bright state, we show how to transfer the squeezing into a dark state

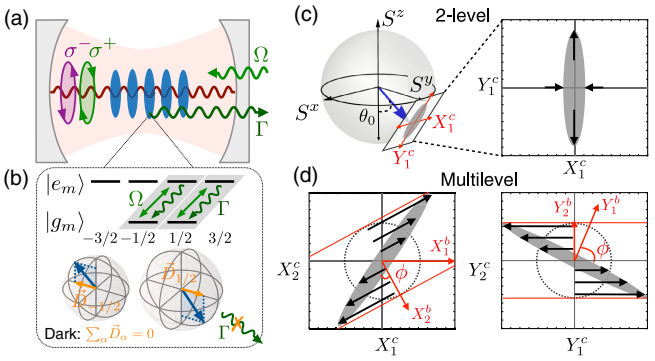

FIG. 1. (a) Atom-cavity setup: Atoms loaded inside a standing-wave cavity, resonant with the atomic transition, decay at a rate Γ. Atoms are coherently driven with right-circularly-polarized light with an effective Rabi frequency Ω. (b) Destructive interference of the collective dipoles $\vec{D}_{\pm 1/2}$ among two transitions in six-level atoms leads to a dark state which does not decay to the ground state. Blue and orange arrows are the mean Bloch vector and dipole for the two transitions. (c) Squeezing in a two-level system, visualized on a Bloch sphere (left) and bosonic noise distribution (right). The steady state is squeezed along $\hat{X}_1^c \propto \hat{S}^x$. (d) Squeezing in a multilevel system. The panels plot projections of the noise distribution onto Schwinger boson quadratures $\hat{X}_{1,2}^c$ and $\hat{Y}_{1,2}^c$, which are proportional to spin variables perpendicular to the multilevel Bloch vector. Black arrows indicate that the distributions shear perpendicular to conserved Bogoliubov bosonic variables $\hat{X}_2^b$ and $\hat{Y}_2^b$ (red arrows), which leads to two squeezed modes.

using single-particle rotations, and store it by using symmetries which preserve quantum noise. The storage protocol can in principle be applied to squeezing generated in multilevel systems via other schemes [23,39–42] such as near-unitary two-mode squeezing in cavities.

The multilevel squeezing can be understood by approximating the spin projections orthogonal to the mean collective spin, to bosonic degrees of freedom (large N expansion). In this picture, multilevel superradiance leads to two-mode squeezing [Fig. 1(d)], in contrast to the one-mode squeezing of two-level atoms [Fig. 1(c)]. This provides an alternative method to produce squeezed states in two independent modes, akin to the two-mode squeezed states realized in BECs and thermal gases [43–51]. Some spin projections are unaffected by superradiance, as suggested by the black arrows in Fig. 1(d), where two specific bosonic quadratures [X_2^b and Y_2^b (red)] are conserved, a property absent from the two-level case. The squeezing can therefore be preserved by rotating the state such that the squeezed quadratures are aligned along the conserved directions.

Setup.—We consider an ensemble of N atoms pinned in a deep magic optical lattice within an optical cavity [see Fig. 1(a)]. For concreteness, we consider atoms with degenerate ground states $|g, m_g\rangle$, $m_g \in [-\frac{1}{2}, \frac{1}{2}]$, and long-lived electronic excited states $|e, m_e\rangle$, $m_e \in [-\frac{3}{2}, \frac{3}{2}]$ and ground-excited transition frequency ω_a, where the quantization axis is along the cavity axis. This can be realized, for example, with the $^1S_0$ and $^3P_1$ states of ^{171}Yb [52]. While our arguments work for generic multilevel atoms, this is the simplest nontrivial atomic structure which shows the relevant physics.

Two cavity modes with angular frequency ω_c and orthogonal polarizations couple ground state atoms to the excited state. For simplicity, we consider that the cavity is resonant with the atoms, $\omega_c = \omega_a = \omega$. We drive the cavity modes with a right-circularly-polarized laser whose frequency is also resonant with the cavity, $\omega_L = \omega$. In the bad cavity limit where the cavity field can be adiabatically eliminated [53], the atom dynamics are described by the Lindblad master equation $\hbar\dot{\rho} = -i[\hat{H}, \rho] + \mathcal{L}[\rho]$ with

$$\hat{H} = \hbar\Omega\hat{D}^x_{+1}, \tag{1}$$

$$\mathcal{L}[\rho] = \hbar\Gamma \sum_{\alpha=\pm1} \left(\hat{D}^-_\alpha \rho \hat{D}^+_\alpha - \frac{1}{2}\{\hat{D}^+_\alpha \hat{D}^-_\alpha, \rho\} \right), \tag{2}$$

where $\{\cdots\}$ is the anticommutator. Equation (1) describes a right-circularly-polarized ($\alpha = +1$) coherent drive, and Eq. (2) describes superradiant emission of left-($\alpha = -1$) and right-circular ($\alpha = +1$) polarizations. Here, Ω is the atoms' effective Rabi coupling strength generated by the drive, and Γ sets the rate at which atoms decay and emit light which leaks out of the cavity. The operator $\hat{D}^+_\alpha = \sum_m C^\alpha_m \hat{S}^+_{m,\alpha}$ describes the collective atomic excitation due to absorbing an α-polarized photon that imparts α units of angular momentum; $\hat{S}^+_{m,\alpha} = \sum_{i=1}^N |e, m+\alpha\rangle_i \langle g, m|_i$ is the collective spin-raising operator for N atoms within the two-level manifold of $|g, m\rangle_i$ and $|e, m+\alpha\rangle_i$; $C^\alpha_m = \langle F_g, m; 1, \alpha | F_e, m+\alpha\rangle$ is the Clebsch-Gordan coefficient for the associated transition; and m is the angular momentum projection of $|g, m\rangle$ onto the quantization axis. We further define $\hat{D}^x_\alpha = [(\hat{D}^+_\alpha + \hat{D}^-_\alpha)/2]$ and $\hat{D}^y_\alpha = [(\hat{D}^+_\alpha - \hat{D}^-_\alpha)/2i]$.

We initialize the atoms in a product of single-particle ground states $|G_\beta\rangle = \cos(\beta/2)|g, -1/2\rangle + \sin(\beta/2)|g, 1/2\rangle$, and apply a right-circularly-polarized pulse to excite a fraction of the atoms to the excited state, leaving them in the coherent state $|\Psi_{\theta_0;\beta}\rangle = |\psi_{\theta_0;\beta}\rangle^{\otimes N} = \exp(-i\theta_0 \hat{D}^x_{+1})|G_\beta\rangle^{\otimes N}$. The levels $|e, -3/2\rangle$ and $|e, -1/2\rangle$ are always empty, so only the right-handed polarization is relevant [Fig. 1(b)]. For convenience, we define a family of states $|\Psi(\theta;\beta)\rangle = \exp(-i\theta\hat{D}^x_{+1})|G_\beta\rangle^{\otimes N}$, with $|\Psi_{\theta_0;\beta}\rangle = |\Psi(\theta_0;\beta)\rangle$.

To study the subsequent evolution it is useful to rewrite the above master equation as $\hbar\dot{\rho} = \mathcal{L}'[\rho]$ where $\mathcal{L}'[\rho]$ looks like $\mathcal{L}[\rho]$ [Eq. (2)] but with the modified jump operators

$$\hat{\mathcal{D}}^-_\alpha = \hat{D}^-_\alpha + i\frac{\Omega_\alpha}{\Gamma}, \tag{3}$$

where $\Omega_{+1} = \Omega$ and $\Omega_{-1} = 0$. One can then show that the system's steady state fulfills $\hat{\mathcal{D}}^-_{+1}\rho_{\rm ss} = 0$ [26,34,35].

Mean-field physics.—A convenient way to visualize the state under the mean-field approximation is in terms of multiple Bloch spheres (labeled m), one for each of the two-level subspaces composed of $|g, m\rangle$ (south pole) and $|e, m+1\rangle$ (north pole), see Fig. 1(b). The dynamics of the mth Bloch vector, $\vec{S}_m = (\langle\hat{S}^x_m\rangle, \langle\hat{S}^y_m\rangle, \langle\hat{S}^z_m\rangle)$, where expectation values are taken in the mean-field state and we dropped the subscript α, is given by [53] $\dot{\vec{S}}_m = C^{+1}_m(\vec{\Omega} + \Gamma\vec{D}_\perp) \times \vec{S}_m$ where $\vec{\Omega} = (\Omega, 0, 0)$ and $\vec{D}_\perp = (-\langle\hat{D}^y_{+1}\rangle, 0, 0)$ for the initial state $|\Psi_{\theta_0;\beta}\rangle$. Therefore, both the Rabi drive and superradiance separately lead to a rotation of each Bloch vector around an axis with fixed direction $\vec{\Omega}/|\vec{\Omega}|$ at a rate $\propto C^{+1}_m$. This means that all Bloch vectors can be described by the single angle $\theta(t)$ as $\vec{S}_m(t) = |\vec{S}_m|(0, \sin[C^{+1}_m\theta(t)], -\cos[C^{+1}_m\theta(t)])$, where $|\vec{S}_m|$ is constant and $\theta(0) = \theta_0$. The mean-field time-evolved state associated with this Bloch vector is $|\Psi(\theta(t);\beta)\rangle$.

The angle $\theta(t)$ evolves according to $\dot{\theta} = \Omega - N\Gamma[\partial V_\beta(\theta)/\partial\theta]$, where $V_\beta(\theta) = \frac{1}{2} + (1/N)\langle\Psi(\theta;\beta)|\sum_m \hat{S}^z_m|\Psi(\theta;\beta)\rangle$ is the superradiance potential [36]. The potential $V_\beta(\theta) = \cos^2(\beta/2)\sin^2(\theta/2\sqrt{3}) + \sin^2(\beta/2)\sin^2(\theta/2)$ is plotted in Fig. 2(a). We can visualize the mean-field dynamics as the classical evolution of a particle with coordinate θ on the potential $V_\beta(\theta)$. Superradiance, which is a form of

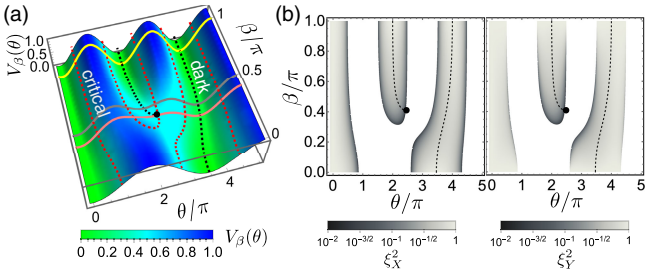

FIG. 2. Superradiance potential $V_\beta(\theta)$. Both height and color indicate $V_\beta(\theta)$, black dashed lines are stable mean-field dark states, and red dashed lines are critical lines. Pink, gray, and yellow lines are parametric cuts explored in this Letter. (b) Steady-state squeezing $\xi^2_{X(Y)}$ in the $\hat{X}$ ($\hat{Y}$) quadratures. The squeezing becomes significant near the critical points [red dashed lines in (a)]. White regions are unstable. The dot indicates where the dark state and critical point coincide.

dissipation, pulls θ towards a minimum of the potential, keeping β fixed, whereas the coherent drive increases (decreases) θ at a constant rate for $\Omega > 0$ ($\Omega < 0$).

The mean-field steady state ($\dot{\theta} = 0$) is given by the solution to $\Omega = N\Gamma[\partial V_\beta(\theta)/\partial\theta]$, when it exists. The stability of this steady state is determined by the curvature of the potential. The steady state is stable to quantum fluctuations for $[\partial^2 V_\beta(\theta)/\partial\theta^2] > 0$, and unstable for $[\partial^2 V_\beta(\theta)/\partial\theta^2] < 0$. The inflection points at $[\partial^2 V_\beta(\theta)/\partial\theta^2]|_{\theta=\theta_c} = 0$ [red dashed lines in Fig. 2(a)] determine critical lines that separate the stable and unstable regions. In the absence of drive, $\Omega = 0$, the steady states are mean-field dark states, and occur when the potential has a minimum with respect to θ [black dashed lines in Fig. 2(a)]. They emerge from destructive interference of the collective dipoles $\vec{D}_m$ in the various Bloch spheres [Fig. 1(b)] [36].

The steady-state solution for θ depends on θ_0, $\Omega/N\Gamma$, and β. For simplicity, we choose throughout the Letter $\Omega = N\Gamma[\partial V_\beta(\theta)/\partial\theta]|_{\theta=\theta_0}$ and $[\partial^2 V_\beta(\theta)/\partial\theta^2]|_{\theta=\theta_0} > 0$. For this choice, the initial state $|\Psi_{\theta_0;\beta}\rangle$ is a stable mean-field steady state. Below the critical points, $|\Psi_{\theta_0;\beta}\rangle$ is a good approximation to the full quantum steady state, and we can treat fluctuations around the mean field as a perturbation.

Quantum noise.—We treat the perturbations around the mean field in a bosonic picture in the large-N approximation. For atoms with ℓ relevant internal levels in the ground and excited manifolds, we can define Schwinger boson operators $\hat{a}_{g(e),m}$ that annihilate particles in $|g(e), m\rangle$, but a more convenient choice turns out to be θ_0-dependent operators $\hat{c}_\mu(\theta_0, \beta)$, $\mu \in [0, \ell - 1]$, that are related to $\hat{a}_{g(e),m}$ via a unitary transformation. For brevity, we will drop the (θ_0, β) dependence of $\hat{c}_\mu$.

We choose the definition of $\hat{c}_\mu$ based on two considerations. First, we define $\hat{c}_{\mu=0}$ to annihilate particles in $|\psi_{\theta_0;\beta}\rangle$. Since we have chosen the initial state $|\Psi_{\theta_0;\beta}\rangle$ to be a mean-field steady state, in the large-N limit we can make the generalized Holstein-Primakoff (HP) approximation [40], $\hat{c}_0 \sim \sqrt{N}$, and assume that the occupation in $|\psi_{\theta_0;\beta}\rangle$ is always close to N. Note that $|\Psi_{\theta_0;\beta}\rangle$ is a macroscopically occupied state of $\hat{c}_0$, and the coherent vacuum for $\hat{c}_{\mu>0}$. The real and imaginary parts of $\hat{c}_{\mu>0}$, $\hat{X}^c_\mu = [(\hat{c}_\mu + \hat{c}^\dagger_\mu)/\sqrt{2}]$ and $\hat{Y}^c_\mu = [(\hat{c}_\mu - \hat{c}^\dagger_\mu)/\sqrt{2}i]$, describe spin variables perpendicular to the Bloch vector (see below). Second, we define $\hat{c}_{\mu>0}$ such that $\hat{\mathcal{D}}^-_{+1}$, which is a linear combination of $\hat{c}_{\mu>0}$, has a simple form [53]. We exemplify this later.

We diagonalize the Lindbladian with a Bogoliubov transformation of $\hat{c}_{\mu>0}$ which defines Bogoliubov bosons $\hat{b}_{\mu>0}$ such that $\hat{\mathcal{D}}^-_{+1} \propto \sqrt{N}\hat{b}_1$. $\hat{b}_\mu$ also depends on (θ_0, β) and we denote their real and imaginary parts as $\hat{X}^b_\mu$ and $\hat{Y}^b_\mu$. This transformation lets us visualize the many-body steady state satisfying $\hat{\mathcal{D}}^-_{+1}\rho_{\rm ss} = 0$, as the vacuum of $\hat{b}_1$. Thus, during the dynamics, the system evolves from the vacuum of $\hat{c}_{\mu>0}$, which has a positive value for $\langle\hat{b}^\dagger_1\hat{b}_1\rangle = \frac{1}{2}[(\Delta X^b_1)^2 + (\Delta Y^b_1)^2 - 1]$, to the vacuum of $\hat{b}_1$, which has $\langle\hat{b}^\dagger_1\hat{b}_1\rangle = 0$ and $(\Delta X^b_1)^2 = (\Delta Y^b_1)^2 = 1/2$, while the $\hat{b}_{1<\mu<\ell}$ bosons remain untouched [Fig. 1(d)]. This noise reduction perpendicular to the Bloch vector corresponds to the generation of spin squeezing.

Specifically, the system is squeezed if some of the spin variables $S_{\perp,\gamma}$ perpendicular to the Bloch vector fulfill $\xi^2_\gamma \equiv 4(\Delta S_{\perp,\gamma})^2/N < 1$. In our approximation, this corresponds to a variance in the $\hat{c}_{\mu>0}$ bosons. We find the smallest variances by calculating the $2(\ell - 1)$ eigenvalues ξ^2_γ of the covariance matrix Σ, whose matrix elements are $\{\langle\{\hat{X}^c_\mu, \hat{X}^c_\nu\}\rangle_C, \langle\{\hat{X}^c_\mu, \hat{Y}^c_\nu\}\rangle_C, \langle\{\hat{Y}^c_\mu, \hat{Y}^c_\nu\}\rangle_C\}$, where $\langle\{\hat{A}, \hat{B}\}\rangle_C = \langle\hat{A}\,\hat{B} + \hat{B}\,\hat{A}\rangle - 2\langle\hat{A}\rangle\langle\hat{B}\rangle$ [53]. Initially, Σ is the identity matrix, which corresponds to no squeezing. As the driven-dissipative system evolves, some eigenvalues of Σ become squeezed, $\xi^2_\gamma < 1$. We show in [53] that an eigenvalue $\xi^2_\gamma < 1$ is an entanglement witness [54,55].

Two-level systems.—To exemplify squeezing in the simplest case, we consider $|G_{\beta=\pi}\rangle = |g, 1/2\rangle$ [yellow line in Fig. 2(a)]. In this case, the dynamics is constrained to $|g, \frac{1}{2}\rangle$ and $|e, \frac{3}{2}\rangle$, effectively realizing a two-level system whose physics has been extensively studied previously [26,27,29–35]. For this case, the superradiance potential is $V_{\beta=\pi}(\theta) = \sin^2(\theta/2)$, whose critical points are $\theta_c = \pm(\pi/2)$. The steady-state Bloch vector is along $\hat{S}^{\rm Bloch}_{\theta_0} = \sin\theta_0\hat{S}^y_{1/2} - \cos\theta_0\hat{S}^z_{1/2}$, stabilized at the mean-field level with a drive strength $\Omega = (N\Gamma/2)\sin\theta_0$ for $|\theta_0| < (\pi/2)$. Defining Schwinger bosons such that [53] $\hat{X}^c_1 \approx \sqrt{(2/N)}\hat{S}^x_{1/2}$ and $\hat{Y}^c_1 \approx \sqrt{(2/N)}(\cos\theta_0\hat{S}^y_{1/2} + \sin\theta_0\hat{S}^z_{1/2})$ in the HP approximation [see Fig. 1(c)], the Lindblad operator can be written as $\hat{\mathcal{D}}^-_{+1} \approx \sqrt{(N/2)}(\hat{X}^c_1 + i\cos\theta_0\hat{Y}^c_1)$. Thus, we define the Bogoliubov operator $\hat{b}_1 = (\hat{X}^c_1/\sqrt{2\cos\theta_0}) + i\hat{Y}^c_1\sqrt{(\cos\theta_0/2)}$, so that $\hat{\mathcal{D}}^-_{+1} = \sqrt{N\cos\theta_0}\hat{b}_1$. Since the

steady state is the vacuum of $\hat{b}_1$ with $(\Delta\hat{X}_1^b)^2 = (\Delta\hat{Y}_1^b)^2 = \frac{1}{2}$, this implies that $\hat{X}_1^c$ and $\hat{Y}_1^c$ are squeezed and antisqueezed in the steady state, respectively, with $(\Delta X_1^c)^2 = (\cos\theta_0/2)$ and $(\Delta Y_1^c)^2 = (1/2\cos\theta_0)$ as shown in Fig. 1(c). The squeezing (antisqueezing) approaches 0 (∞) as θ_0 approaches the critical point, $\theta_c = \pm(\pi/2)$.

Multilevel systems.—When both ground levels are initially populated, the system hosts four nontrivial Schwinger bosons $\hat{c}_\mu$ and thus three Bogoliubov bosons $\hat{b}_\mu$. We define $\hat{c}_\mu$ such that the jump operator is [53]

$$\hat{D}_{+1}^{-} \approx \sqrt{N}\left(x\hat{X}_1^c + iy(\cos\phi\hat{Y}_1^c + \sin\phi\hat{Y}_2^c)\right), \qquad (4)$$

where (x, y, ϕ) are parameters that depend on (θ_0, β). Specifically, *all* the critical points, $[\partial^2 V_\beta(\theta)/\partial\theta^2]|_{\theta=\theta_0} = 0$, correspond to $\phi = (\pi/2)$. As before, we define $\hat{b}_1$ via $\hat{D}_{+1}^{-} \approx \sqrt{Nxy\cos\phi}\hat{b}_1$. We define the other two Bogoliubov operators as $\hat{b}_2 = \{[(\hat{X}_2^c - \tan\phi\hat{X}_1^c) + i\hat{Y}_2^c]/\sqrt{2}\}$ and $\hat{b}_3 = \hat{c}_3$. These modes commute with $\hat{D}_{+1}^{\pm}(\propto \hat{b}_1, \hat{b}_1^\dagger)$, and therefore their quadratures are conserved during dynamics. $\hat{b}_2$ and $\hat{b}_3$ are said to be generators of strong symmetries [56–59].

The evolution relaxes the system to the vacuum of $\hat{b}_1$, which leads to dynamics in $\hat{c}_1$ and $\hat{c}_2$ only. The $\hat{b}_3$ boson thus plays no role in the dynamics. However, since $\hat{b}_2$ is conserved, the dynamics in $\hat{c}_1$ and $\hat{c}_2$ is such that the noise distributions shear perpendicular to $\hat{X}_2^b$ and $\hat{Y}_2^b$, as shown in Fig. 1(d). This shearing leads to squeezing in *two distinct modes* in the $\hat{c}$ basis, one in the X_1^c-X_2^c plane and one in the Y_1^c-Y_2^c plane, as opposed to the single squeezed mode of the two-level system above. The shearing is reminiscent of spin squeezing via, e.g., one-axis twisting (OAT). Unlike OAT, however, the dissipative dynamics does not preserve the area of the noise distribution, and also the shearing rate is time dependent and stops when $(\Delta X_1^b)^2 = (\Delta Y_1^b)^2 = \frac{1}{2}$.

Figure 2(b) plots the squeezing in the two squeezed modes. The squeezing in both modes approaches 0 at the critical lines ($\phi = \pi/2$), but finite-N effects limit the best squeezing achievable. Near the critical point, the squeezed quadratures approach $\hat{X}_1^c$, which is $\propto \hat{D}_{+1}^x$, and $\hat{Y}_2^c$, which is $\propto \hat{D}_{+1}^y - \langle\hat{D}_{+1}^y\rangle$ [53].

Squeezing in a dark state.—The simplest way to generate scalable squeezing in a dark state is to initially prepare the system in a mean-field dark state that is close to a critical point, and let the system evolve with $\Omega = 0$. We achieve this by choosing β and θ_0 appropriately. Figure 2(a) shows that the dark manifold (black dashed line) intersects the critical manifold (red dashed line) at a saddle point (black dot) given by $(\theta_{c,\mathrm{dark}}, \beta_{c,\mathrm{dark}}) \approx (2.45\pi, 0.41\pi)$ [53]. To avoid finite-N effects, we can work at a slightly larger β, e.g., $\beta = 0.411\pi$, whose superradiance potential is shown in Fig. 3(a) and as a pink line in Fig. 2(a). The potential has a dark state at $(\theta_0, \beta) = (2.41\pi, 0.411\pi)$, which is close to the critical point at $\theta_c = 2.45\pi$. Preparing

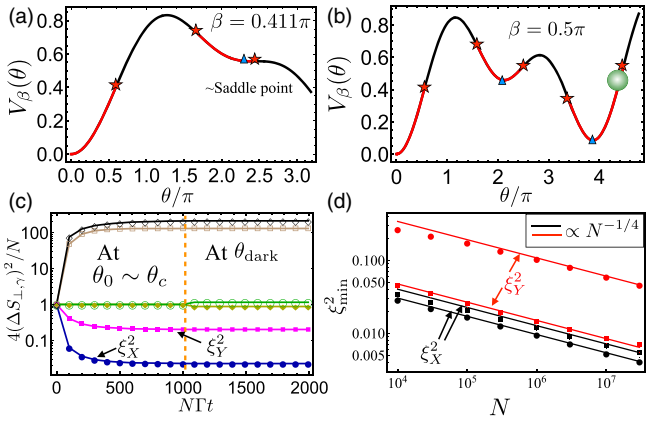

FIG. 3. (a),(b) Superradiance potential $V_\beta(\theta)$ at (a) $\beta = 0.41\pi$ and (b) $\beta = 0.5\pi$. Blue triangles and red stars indicate dark states and critical points respectively. (c) The six leading eigenvalues of the spins' covariance matrix $\tilde{\Sigma}$ during the storage protocol at $(\theta_0, \beta) = (4.46\pi, 0.5\pi)$, calculated using a cumulant expansion truncated at second order [53]. These eigenvalues correspond to the six normalized variances, $4(\Delta S_{\perp,\gamma}^2)/N$, of the spin variables perpendicular to the Bloch vector. The two squeezed modes preserve the noise after rotating to the dark state at $t = 1000/(N\Gamma)$. Lines are guides to the eye. (d) Finite-size scaling of the best squeezing in the $\hat{X}$ and $\hat{Y}$ quadratures near the critical points $(\theta_c, \beta) = (4.47\pi, 0.5\pi)$ (dots) and $(\theta_{c,\mathrm{dark}}, \beta_{c,\mathrm{dark}}) = (2.45\pi, 0.41\pi)$ (squares).

the system at this value of (θ_0, β) will yield $\xi^2 \sim 0.05$ without any driving. This squeezing gets better as the critical point $(\theta_{c,\mathrm{dark}}, \beta_{c,\mathrm{dark}}) \approx (2.45\pi, 0.41\pi)$ is approached.

Transferring the squeezing to the dark state.—Scalable squeezing can also be generated with $\Omega \neq 0$ in a bright state close to other critical points. This squeezing can still be transferred to a dark state, θ_{dark}, where it will be immune to superradiance after switching off the drive. This idea works regardless of how the squeezing was generated as long as the HP approximation is valid.

As an example, we consider spin squeezing generated at $(\theta_0, \beta) = (4.46\pi, 0.5\pi)$ [green circle in Fig. 3(b)], where θ_0 is close to a critical point, $\theta_c = 4.47\pi$ [Fig. 3(b) and gray cut in Fig. 2(a)]. The basic idea, after acquiring squeezing in a bright state, is to first rotate the Bloch vector to a mean-field dark state and switch off the continuous drive Ω. This can be accomplished by a rotation $\exp[i(\theta_0 - \theta_{\mathrm{dark}})\hat{D}_{+1}^x]$ to the dark state at $\theta_{\mathrm{dark}} = 3.87\pi$. Then, to avoid losing the squeezing due to further evolution towards the new steady state at θ_{dark} and $\Omega = 0$, one needs to perform additional single-particle rotations that transfer the squeezed quadratures to the conserved quadratures $\hat{X}_2^b$, $\hat{X}_3^b$, $\hat{Y}_2^b$, or $\hat{Y}_3^b$. Explicit forms of these rotations are given in [53]. Single-particle rotations for multilevel atoms can be implemented using, e.g., quantum optimal control [60]. Note that all rotations should be fast compared to $N\Gamma$.

We numerically simulate this protocol using a cumulant expansion [53] in Fig. 3(c), which shows the evolution of

the noise (variances of spin variables) for $(\theta_0, \beta) = (4.46\pi, 0.5\pi)$. At $t = (1000/N\Gamma)$ we implement the above rotations and let the system evolve freely with $\Omega = 0$. Clearly, the two most squeezed quadratures are preserved.

Best squeezing achievable.—The best squeezing achieved is limited by higher-order terms in the HP approximation, and single-particle decoherence set fundamentally by the single-particle linewidth γ. In Fig. 3(d), we use the cumulant expansion, which includes the higher-order HP corrections, to find the best squeezing in the two modes for the two above protocols: squeezing at a dark state or a bright state. Specifically, we scan θ_0 between 2π and 2.45π along the dark manifold [dashed black line in Fig. 2(b)], and θ_0 between 3.87π and 4.47π at $\beta = 0.5\pi$ [Fig. 3(b)]. We numerically find in all cases that the squeezing ξ^2 scales as $N^{-0.25}$, and derive this scaling in [53]. We show in [53] that free-space spontaneous emission yields squeezing which scales with N as $1/\sqrt{NC}$ where $C = \Gamma/\gamma$ is the cavity cooperativity. For $NC^2 \gg 1$, finite-size effects limit the squeezing more than spontaneous emission. Our protocol has the advantage that squeezing is generated in more than one quadrature and is thus useful for more general metrological tasks [61].

Outlook.—While we have focused on the case with only one relevant polarization, the ideas presented can be generalized to situations with two relevant polarizations, where up to four quadratures can be squeezed [53]. The presented ideas open unique opportunities for the generation and storage of squeezing in generic multilevel systems even beyond the cavity setting discussed here.

We thank Jeremy T. Young, Dylan Young, and James K. Thompson for valuable discussions and carefully reading the manuscript. This work is supported by the AFOSR Grants No. FA9550-18-1-0319 and No. FA9550-19-1-0275, by the DARPA and ARO Grant No. W911NF-16-1-0576, by the NSF JILA-PFC PHY-2317149, QLCI-OMA-2016244, by the U.S. Department of Energy, Office of Science, National Quantum Information Science Research Centers Quantum Systems Accelerator, the Vannevar Bush Faculty Fellowship, and by the National Institute of Standards and Technology.

*Present address: Rigetti Computing, Berkeley, California 94710, USA.

[1] R. H. Dicke, Coherence in spontaneous radiation processes, Phys. Rev. **93**, 99 (1954).
[2] A. Asenjo-Garcia, M. Moreno-Cardoner, A. Albrecht, H. J. Kimble, and D. E. Chang, Exponential improvement in photon storage fidelities using subradiance and "selective radiance" in atomic arrays, Phys. Rev. X **7**, 031024 (2017).
[3] E. Shahmoon, D. S. Wild, M. D. Lukin, and S. F. Yelin, Cooperative resonances in light scattering from two-dimensional atomic arrays, Phys. Rev. Lett. **118**, 113601 (2017).
[4] J. Rui, D. Wei, A. Rubio-Abadal, S. Hollerith, J. Zeiher, D. M. Stamper-Kurn, C. Gross, and I. Bloch, A subradiant optical mirror formed by a single structured atomic layer, Nature (London) **583**, 369 (2020).
[5] J. A. Needham, I. Lesanovsky, and B. Olmos, Subradiance-protected excitation transport, New J. Phys. **21**, 073061 (2019).
[6] K. E. Ballantine and J. Ruostekoski, Subradiance-protected excitation spreading in the generation of collimated photon emission from an atomic array, Phys. Rev. Res. **2**, 023086 (2020).
[7] J. Perczel, J. Borregaard, D. E. Chang, H. Pichler, S. F. Yelin, P. Zoller, and M. D. Lukin, Topological quantum optics in two-dimensional atomic arrays, Phys. Rev. Lett. **119**, 023603 (2017).
[8] J. Perczel, J. Borregaard, D. E. Chang, H. Pichler, S. F. Yelin, P. Zoller, and M. D. Lukin, Photonic band structure of two-dimensional atomic lattices, Phys. Rev. A **96**, 063801 (2017).
[9] R. J. Bettles, J. Minar, C. S. Adams, I. Lesanovsky, and B. Olmos, Topological properties of a dense atomic lattice gas, Phys. Rev. A **96**, 041603(R) (2017).
[10] A. Zhang, X. Chen, V. V. Yakovlev, and L. Yuan, Tunable topologically-protected super-and subradiant boundary states in one-dimensional atomic arrays, Commun. Phys. **2**, 157 (2019).
[11] S. V. Syzranov, M. L. Wall, B. Zhu, V. Gurarie, and A. M. Rey, Emergent Weyl excitations in systems of polar particles, Nat. Commun. **7**, 13543 (2016).
[12] A. González-Tudela, V. Paulisch, D. E. Chang, H. J. Kimble, and J. I. Cirac, Deterministic generation of arbitrary photonic states assisted by dissipation, Phys. Rev. Lett. **115**, 163603 (2015).
[13] L. Henriet, J. S. Douglas, D. E. Chang, and A. Albrecht, Critical open-system dynamics in a one-dimensional optical-lattice clock, Phys. Rev. A **99**, 023802 (2019).
[14] C. Qu and A. M. Rey, Spin squeezing and many-body dipolar dynamics in optical lattice clocks, Phys. Rev. A **100**, 041602(R) (2019).
[15] A. Piñeiro Orioli and A. M. Rey, Dark states of multilevel fermionic atoms in doubly filled optical lattices, Phys. Rev. Lett. **123**, 223601 (2019).
[16] A. Piñeiro Orioli and A. M. Rey, Subradiance of multilevel fermionic atoms in arrays with filling $n \geq 2$, Phys. Rev. A **101**, 043816 (2020).
[17] J. Ma, X. Wang, C.-P. Sun, and F. Nori, Quantum spin squeezing, Phys. Rep. **509**, 89 (2011).
[18] M. H. Schleier-Smith, I. D. Leroux, and V. Vuletić, Squeezing the collective spin of a dilute atomic ensemble by cavity feedback, Phys. Rev. A **81**, 021804(R) (2010).
[19] I. D. Leroux, M. H. Schleier-Smith, and V. Vuletić, Implementation of cavity squeezing of a collective atomic spin, Phys. Rev. Lett. **104**, 073602 (2010).
[20] Z. Chen, J. G. Bohnet, J. M. Weiner, K. C. Cox, and J. K. Thompson, Cavity-aided nondemolition measurements for atom counting and spin squeezing, Phys. Rev. A **89**, 043837 (2014).
[21] K. C. Cox, G. P. Greve, J. M. Weiner, and J. K. Thompson, Deterministic squeezed states with collective measurements and feedback, Phys. Rev. Lett. **116**, 093602 (2016).

[22] O. Hosten, N. J. Engelsen, R. Krishnakumar, and M. A. Kasevich, Measurement noise 100 times lower than the quantum-projection limit using entangled atoms, Nature (London) **529**, 505 (2016).
[23] L. Pezzè, A. Smerzi, M. K. Oberthaler, R. Schmied, and P. Treutlein, Quantum metrology with nonclassical states of atomic ensembles, Rev. Mod. Phys. **90**, 035005 (2018).
[24] M. Gross and S. Haroche, Superradiance: An essay on the theory of collective spontaneous emission, Phys. Rep. **93**, 301 (1982).
[25] M. A. Norcia, M. N. Winchester, J. R. K. Cline, and J. K. Thompson, Superradiance on the millihertz linewidth strontium clock transition, Sci. Adv. **2**, e1601231 (2016).
[26] D. Barberena, R. J. Lewis-Swan, J. K. Thompson, and A. M. Rey, Driven-dissipative quantum dynamics in ultra-long-lived dipoles in an optical cavity, Phys. Rev. A **99**, 053411 (2019).
[27] E. Wolfe and S. F. Yelin, Spin squeezing by means of driven superradiance, arXiv:1405.5288.
[28] E. G. Dalla Torre, J. Otterbach, E. Demler, V. Vuletic, and M. D. Lukin, Dissipative preparation of spin squeezed atomic ensembles in a steady state, Phys. Rev. Lett. **110**, 120402 (2013).
[29] D. F. Walls, P. D. Drummond, S. S. Hassan, and H. J. Carmichael, Non-equilibrium phase transitions in cooperative atomic systems, Prog. Theor. Phys. Suppl. **64**, 307 (1978).
[30] P. D. Drummond and H. J. Carmichael, Volterra cycles and the cooperative fluorescence critical point, Opt. Commun. **27**, 160 (1978).
[31] P. D. Drummond and S. S. Hassan, Multiple sidebands in cooperative resonance fluorescence: Exact semiclassical results, Phys. Rev. A **22**, 662 (1980).
[32] P. D. Drummond, Observables and moments of cooperative resonance fluorescence, Phys. Rev. A **22**, 1179 (1980).
[33] H. J. Carmichael, Analytical and numerical results for the steady state in cooperative resonance fluorescence, J. Phys. B **13**, 3551 (1980).
[34] R. R. Puri and S. V. Lawande, Exact steady-state density operator for a collective atomic system in an external field, Phys. Lett. A **72**, 200 (1979).
[35] O. Somech and E. Shahmoon, Quantum entangled states of a classically radiating macroscopic spin, arXiv:2204.05455.
[36] A. Piñeiro Orioli, J. K. Thompson, and A. M. Rey, Emergent Dark states from superradiant dynamics in multilevel atoms in a cavity, Phys. Rev. X **12**, 011054 (2022).
[37] R. Lin, R. Rosa-Medina, F. Ferri, F. Finger, K. Kroeger, T. Donner, T. Esslinger, and R. Chitra, Dissipation-engineered family of nearly dark states in many-body cavity-atom systems, Phys. Rev. Lett. **128**, 153601 (2022).
[38] J. Fan and S. Jia, Collective dynamics of the unbalanced three-level Dicke model, Phys. Rev. A **107**, 033711 (2023).
[39] L. M. Norris, C. M. Trail, P. S. Jessen, and I. H. Deutsch, Enhanced squeezing of a collective spin via control of its qudit subsystems, Phys. Rev. Lett. **109**, 173603 (2012).
[40] Z. Kurucz and K. Mølmer, Multilevel Holstein-Primakoff approximation and its application to atomic spin squeezing and ensemble quantum memories, Phys. Rev. A **81**, 032314 (2010).
[41] S. J. Masson, M. D. Barrett, and S. Parkins, Cavity QED Engineering of spin dynamics and squeezing in a spinor gas, Phys. Rev. Lett. **119**, 213601 (2017).
[42] B. Sundar, D. Barberena, A. Piñeiro Orioli, A. Chu, J. K. Thompson, A. M. Rey, and R. J. Lewis-Swan, Bosonic pair production and squeezing for optical phase measurements in long-lived dipoles coupled to a cavity, Phys. Rev. Lett. **130**, 113202 (2023).
[43] C. Gross, H. Strobel, E. Nicklas, T. Zibold, N. Bar-Gill, G. Kurizki, and M. K. Oberthaler, Atomic homodyne detection of continuous-variable entangled twin-atom states, Nature (London) **480**, 219 (2011).
[44] B. Lücke, M. Scherer, J. Kruse, L. Pezzé, F. Deuretzbacher, P. Hyllus, J. Peise, W. Ertmer, J. Arlt, L. Santos, A. Smerzi, and C. Klempt, Twin matter waves for interferometry beyond the classical limit, Science **334**, 773 (2011).
[45] E. M. Bookjans, C. D. Hamley, and M. S. Chapman, Strong quantum spin correlations observed in atomic spin mixing, Phys. Rev. Lett. **107**, 210406 (2011).
[46] A. T. Black, E. Gomez, L. D. Turner, S. Jung, and P. D. Lett, Spinor dynamics in an antiferromagnetic spin-1 condensate, Phys. Rev. Lett. **99**, 070403 (2007).
[47] L. Zhao, J. Jiang, T. Tang, M. Webb, and Y. Liu, Dynamics in spinor condensates tuned by a microwave dressing field, Phys. Rev. A **89**, 023608 (2014).
[48] A. Qu, B. Evrard, J. Dalibard, and F. Gerbier, Probing spin correlations in a Bose-Einstein condensate near the single-atom level, Phys. Rev. Lett. **125**, 033401 (2020).
[49] K. Kim, J. Hur, S. J. Huh, S. Choi, and J.-y. Choi, Emission of spin-correlated matter-wave jets from spinor Bose-Einstein condensates, Phys. Rev. Lett. **127**, 043401 (2021).
[50] B. Julsgaard, A. Kozhekin, and E. S. Polzik, Experimental long-lived entanglement of two macroscopic objects, Nature (London) **413**, 400 (2001).
[51] E. S. Polzik and J. Ye, Entanglement and spin squeezing in a network of distant optical lattice clocks, Phys. Rev. A **93**, 021404(R) (2016).
[52] A. D. Ludlow, M. M. Boyd, J. Ye, E. Peik, and P. O. Schmidt, Optical atomic clocks, Rev. Mod. Phys. **87**, 637 (2015).
[53] See Supplemental Material at http://link.aps.org/supplemental/10.1103/PhysRevLett.132.033601 for derivations of master equation, mean-field physics, squeezing, transfering the squeezing, and numerical benchmarks, which includes Ref. [54].
[54] G. Vitagliano, P. Hyllus, I. L. Egusquiza, and G. Tóth, Spin squeezing inequalities for arbitrary spin, Phys. Rev. Lett. **107**, 240502 (2011).
[55] G. Vitagliano, I. Apellaniz, I. L. Egusquiza, and G. Tóth, Spin squeezing and entanglement for an arbitrary spin, Phys. Rev. A **89**, 032307 (2014).
[56] S. Lieu, R. Belyansky, J. T. Young, R. Lundgren, V. V. Albert, and A. V. Gorshkov, Symmetry breaking and error correction in open quantum systems, Phys. Rev. Lett. **125**, 240405 (2020).
[57] T. Prosen, Third quantization: A general method to solve master equations for quadratic open fermi systems, New J. Phys. **10**, 043026 (2008).

[58] B. Buča and T. Prosen, A note on symmetry reductions of the Lindblad equation: Transport in constrained open spin chains, New J. Phys. **14**, 073007 (2012).

[59] T. Barthel and Y. Zhang, Solving quasi-free and quadratic Lindblad master equations for open fermionic and bosonic systems, J. Stat. Mech. (2022) 113101.

[60] S. Omanakuttan, A. Mitra, M. J. Martin, and I. H. Deutsch, Quantum optimal control of ten-level nuclear spin qudits in sr 87, Phys. Rev. A **104**, L060401 (2021).

[61] L. Pezzè, A. Smerzi, M. K. Oberthaler, R. Schmied, and P. Treutlein, Quantum metrology with nonclassical states of atomic ensembles, Rev. Mod. Phys. **90**, 035005 (2018).